MODELLING LOADING AND BREAK-UP OF RC STRUCTURE DUE TO INTERNAL EXPLOSION OF FRAGMENTING SHELLS

J. Weerheijm[1,3], A.Stolz[2] , W.Riedel[2], J.Mediavilla[1]

[1]*TNO Defence Security and Safety, PO Box 45, 2280 AA Rijswijk, The Netherlands*
[2]*Ernst Mach Institute, Eckerstraße 4, 79104 Freiburg, Germany*
[3]*Delft University of Technology, The Netherlands*

Abstract

The Klotz Group (KG), an international group of experts on explosion safety, investigates the debris throw hazard associated with the accidental detonation of ammunition in reinforced concrete (RC-) structures. Experiments are combined with engineering models but also with results of advanced computational modeling, which is the topic of this paper. EMI and TNO are establishing a three step approach to analyze the explosion phenomena of single and multiple bare and cased charges in a RC-structure. In the first step the blast loading and gas pressure is computed including the venting process. A cubicle RC structure was modeled in 3D to capture the correct structural failure mode and venting process, from the coupled fluid-structure interaction simulations. The second step consists of internal trajectory predictions using fragmentation matrices based on arena test data together with hydrocode simulations for deeper understanding the jetting effects of casing remainders within the concrete housing. The predicted blast and fragment loads are the input for the third step on the dynamic response and break-up of the structure. In this step the structure was modeled with a simulation approach to capture the local failure phenomena and final break-up as good as possible.

The approach was applied on a series of explosion tests with cased and uncased charges. The simulations predicted higher velocities, higher kinetic and higher internal energy for the bare charge tests, while the impulse at the wall is higher for the shell tests. The predicted debris launch conditions are in good agreement with the test results, which exhibited clear differences between bare and cased charges. Evidently, the spatial and temporal load distributions have a significant effect on the failure of the structure. The simulations provide the information to interpret the test data correctly and allow to derive simple casing influence factor for available engineering approaches.
The results of this three step approach are promising in spite of the fact that the currently available commercial codes and numerical (material) models have to used to the limit of applicability with the extreme conditions of explosive loading and full break-up of the RC-structure. In the paper we will present and discuss the computational strategy and the comparison of numerical predictions with available test results.

Keywords: *Numerical modeling – Explosion – Fragments Venting – Concrete break-up*

Introduction

Shell ammunition is often stored in stacks inside reinforced concrete magazines. Although high security measures are in place is most cases an explosion may always occur. The blast, fragments and magazine debris are the external explosion effects. The Klotz Group, an international group of experts on explosion safety, investigates these hazards with a special focus on the debris throw. Experiments are combined with engineering models but also with results of advanced computational modeling which is the topic of this paper.

Hitherto, regulations and debris throw models are mainly based on bare charge data. In 2008 the KG started an experimental and theoretical study on the break-up of RC-structures due to the explosion of fragmenting shells. This study aims at getting (i) data on debris mass distribution and throw distance that can be compared with and related to the data for bare charge detonation and (ii) a better physical understanding of the break-up and mass distribution of reinforced concrete ammunition storage buildings and the effect of the fragmenting shells on this response. This paper is concerned with the theoretical and the numerical aspects of this KG-research.

EMI and TNO established a three step approach to analyze the explosion phenomena of single and multiple bare and cased charges in a RC-structure. In the first step the blast loading and gas pressure insided the housing is modeled including the venting process. The cubicle RC-structure is modeled in 3D to capture the correct structural failure mode and venting process, from the coupled fluid-structure interaction simulations. The second step consists of shell debris trajectory predictions using fragmentation matrices based on arena test data together with hydrocode simulations for deeper understanding the jetting effects within the stacks. The predicted blast and fragment loads are the input for the third step on the dynamic response and break-up of the structure. In this step the structure is modeled with a simulation approach that captures the local failure phenomena and final break-up as good as possible. This three-step – approach is illustrated in **Figure 1**.

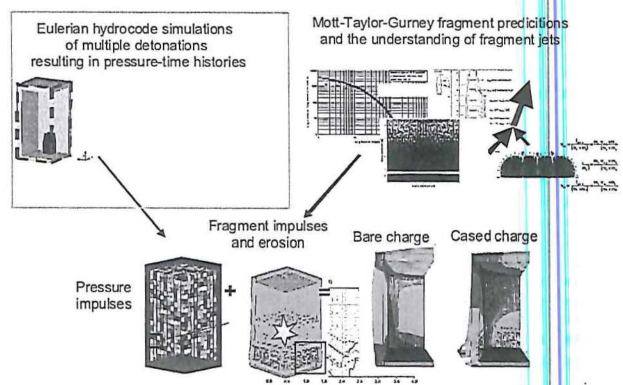

Figure 1 The KG- three step simulation approach to derive internal blast pressures (upper left, FEM), fragment trajectories (upper right, analytical) onto the concrete housing (lower center, FEM)

The structure of the paper is as follows. First the experiments are summarized as background for the application and requirements for the numerical modeling. The three modeling steps are presented and discussed in the next chapters. After that the numerical results are compared with the experimental data and conclusions are drawn.

Experimental program

In addition to existing data on small and full scale explosion tests with above ground ammunition magazines, the KG started in 2008 a systematic study on the break-up of a RC-structure type that was in use in Norway and Sweden for small amounts of ammunition. Data collection occurs according to an internationally agreed standard. The so called "Kasun" RC-structure has a cubical shape with internal dimensions of $2x2x2$ m^3 with a wall and roof thicknesses of 0.15 m and is made of concrete B35. The structure is double reinforced in both directions with an external concrete cover of 25 mm, and an internal concrete cover of 20 mm. The rebar diameter is 12 mm and the spacing is 100 mm. The reinforcement is FeB400. The door opening is 900 mm x 1700 mm, but is not considered in the study.

The test structure is situated in a flat, obstacle-free area for debris collection. Debris is collected up to 500 meters for mass classes ranging from 10 grams up to remainders larger than 24 kg. The debris throw is recorded using high speed cameras in parallel to internal and external blast measurements. An additional set of high speed cameras was applied to record the initial response mode of the structure and the debris throw pattern. The test program consisted of bare and fragmenting shells. The test scheme is summarized in Table 1. The ratio of the charge weight and the structure volume is also given, because it is a key loading parameter in existing engineering approaches and indicator for the kind of response and failure mode of the RC-structure. The Kasun structure and the stack configuration of 16 shells are given in **Figure 2**.

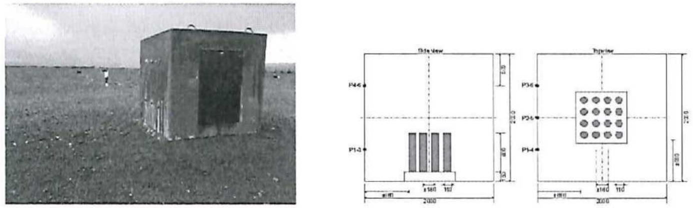

Figure 2 (left) Instrumented Kasun test structure on test field; (right) and stack configuration for 16 shells

Table 1 Test program ranging from low to high loading densities with bare and cased charges

Charge type	Charge weight (kg TNT equ)	Loading density (kg TNT/m^3)
Bare	6.9	0.86
Bare	110	13.8
1 shell	6.9	0.86
4 shells	27.9	3.50
16 shells	110	13.8

The numerical model: Step 1 Internal blast load

2.1. Introduction

In the numerical modeling we follow the sequential steps of the explosion process. First we have to deal with the detonation of the explosives and the generated and expanding explosion products. For this initial phase a high resolution flow domain is defined. Afterwards the energy is transferred to the surrounding air. The blast expands and multiple reflections of the shock wave occur at the walls, ceiling and floor. For this phase the required resolution of the grid needed to capture the dominant effects is lower than in the high definition zone directly around the charge. At the same time, the fluid-structure coupling with the surrounding housing is slowing down computational speed by an order of magnitude. The flow domain is extended outside the structure to capture the venting process when the structure starts to expand and fails due to the multiple shockwaves and the generated quasi-static overpressure (see Figure 3 and section 2.2). To predict the loading on the structure itself we need – although coarser than in step 3 - a sufficiently detailed structural response model to capture the failure mode and get the timing in the whole loading process correct (see section 2.3).

In the blast prediction for the cased charges the failure of the casing has to be included. A part of the explosion energy is absorbed by the fragmentation. The formation of the expanding blast waves is some what delayed and jetting effects occur. This part of the modeling is done in the high resolution flow domain and discussed in 2.2.

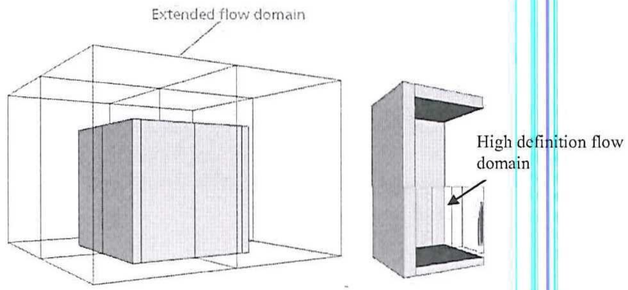

Figure 3 Schematic view of the two flow domains. (left) The extended flow domain to capture the loading on the structure and the venting process and (right) the high definition domain to capture initial phase.

2.2. Detonation of bare and cased charges

As mentioned in the previous section, the detonation of the charge is calculated in a high resolution flow domain with an element size of 5 mm. To ensure that the mesh is fine enough for the detonation process of the explosive, two-dimensional axial symmetric simulations had been carried out using the well quantified blast loading from a spherical charge. In these simulations, a spherical explosive mass was discretized with the same resolution used for the 3D ammunition simulation in the KASUN house model. The calculated peak overpressure and impulses correspond with the empirical values given by Kingery and Bulmash.

The explosive charge and casing are modeled with a very fine grid (5 mm) as depicted in Figure 4.

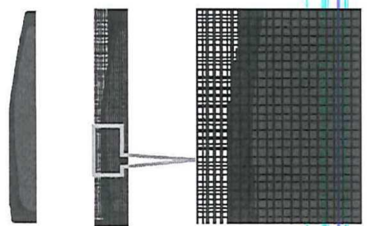

Figure 4 Mesh size of the explosive and the ammunition shell in the Eulerian flow domain.

The resolution of the first step is used until the explosive is fully detonated, the structural resistance of the casing has ended and the shock almost reaches the boundaries of the first flow domain (see Figure 3). The latter determines the size of the required first, high definition flow domain. At that point the mesh coarsened and remapped to an element edge size of 25 mm in each direction, see Figure 5. In order to study and quantify the effect of cased ammunition versus bare explosives to the break-up and debris throw, it is important to include the effect of the casing fragmentation on the blast loading.

structure was built. The requirement was that the failure modes and time for the loading (single charge up to 16 charges) as well as the beginning venting through the breaking walls could be represented. The concrete structure was modeled with 8-nodes first order solid elements of 25 mm and the RHT concrete model [1, 5]. The two layers of reinforcement bars were modeled as discrete beam elements (see Figure 8) in full scale without any simplifications. Note that the element size of 25 mm corresponds to the grid size of the flow domain.

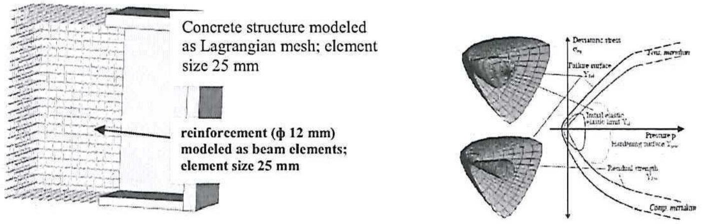

Figure 8 The KASUN structural response model (left) and the RHT concrete model (right).

Numerical modeling of complete failure leads easily to severely decreasing time steps when the Lagrangean mesh distortion is too large. To overcome this problem and in order to simulate on a phenomemnological level the venting between originating concrete fragments, elements are eroded at a critical deformation level. It was decided to use the high speed recordings of the venting onset in the KASUN tests to determine the critical strain to be used as "erosion criterion" for this problem. In [5] the calibration procedure is described extensively, here we just summarize.

First, the simulation was evaluated by the comparison of the numerical results to the high speed video frames at certain times for the 1 bare charge configuration at three moments. Figure 9 shows synchronized simulation results and high speed recordings. The red clouds in the simulations represent the detonation products. Various critical strain values have been used in the evaluation. For all three time steps an erosion criteria of 50 % geometric strain produced the best results in terms of onset location and amount of venting. The areas where the structure breaks open are in good congruence to the experimental observations, even if the calculated destruction of the structure seems to be slightly too low in the numerical model, especially in the bottom corner region of the housing. Comparing high speed frames and the numerical data one has to keep in mind that not all the visible clouds have to be blasting fume, but can also be dust clouds. The analysis of regions which are not eroded completely at these time step showed that the deformations in these regions almost meet the erosion strain criterion. From these evaluations is has been concluded that the 50% strain seems to be an appropriate erosion criterion. To confirm this, also the other loading densities have been analyzed. For the 4 shell and 16 shell configuration the chosen 50% strain criteria provided very good results as well as for the location of the area which fails and the magnitude of the eroded area for all regarded time steps(see figure 10). Also the comparison of the numerical results and the test high speed videos for the 16 bare charges presents good agreement. In this case the eroded areas seem to be a little bit too large in the numerical simulation

Figure 10 shows effect of the erosion strain on the resulting transient pressure and impulse courses measured at one gauge point in the center of the wall region for the lowest bare charge density. The solid black line represents the calculations with a standard high erosion strain (200%) often used for the investigations of penetration problems. The dotted line gives the results accomplished with the 50% erosion strain, which showed good agreement with the video images of the experiments. Comparing the two curves the first peak overpressure shows no significant difference between the two calculations but in time the two pressure courses diverge due to the different erosion strain. The calculated pressure for the lower erosion strain results in significantly lower pressures and impulses on a longer runtime.

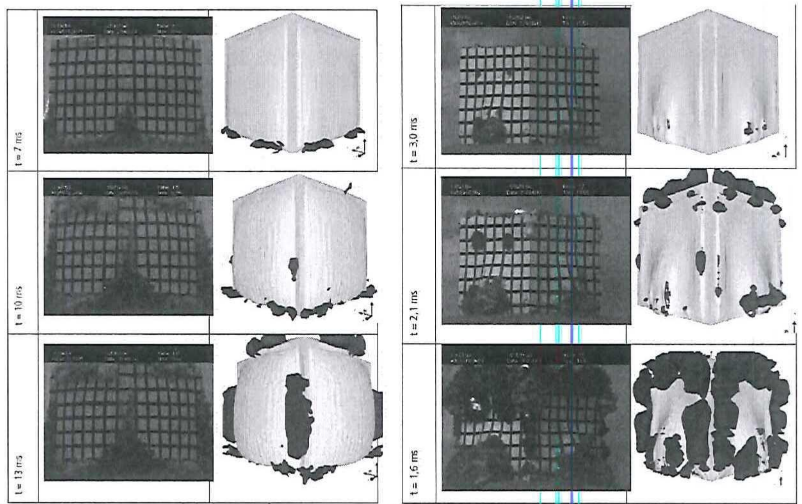

Figure 9 Comparison of failure mode and timing of the numerical load and response model with the high speed KASUN trial recordings. Erosion criterion: 50% geometric strain. (left) single bare charge . (right) 16 shells test.

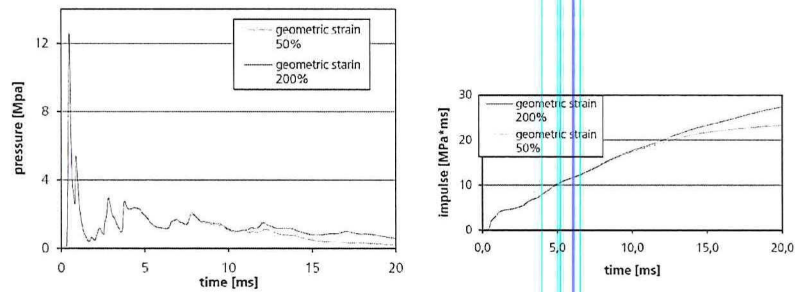

Figure 10 (left) pressure time at centre of wall (1 bare charge); (right) the impulse-time curves

These phenomena can also be clearly identified in the impulse curves. The standard 200% erosion strain generates for the examined gauge point an at least 10% higher impulses due to the detonation. In addition it can be noted that for the 50%, the asymptote of the impulse curve is almost reached after 20 milliseconds, while for the 200% criterion the impulse is still

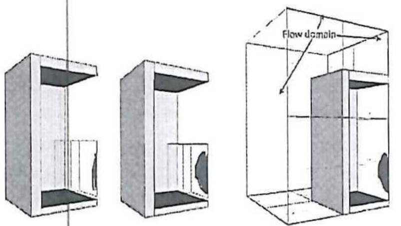

Figure 5 Detonation of the ammunition in a small, high definition flow domain (left and middle); Coarsened remeshing and extended flow domain (right).

For the numerical simulations some simplifications have to be made to create a system which can be solved with a reasonable computational effort. The cased and uncased ammunition masses have been discretized in an Eulerian-Multi-Material mesh domain using an Euler-Godunov solver scheme. To represent the structural behavior of the casing, the mesh resolution is adjusted so that the casing is subdivided in more than two elements over the thickness of the steel casing. The material behavior is described using a Johnson-Cook material model, neglecting the possible strain rate and temperature related effects on the strength of the material. The yield stress of the B125 steel is 350 MPa, the ultimate strength 750 MPa and the maximum failure strain is 15 %.

In order to check the suitability of the approach the results have been compared to additional simulations of the casing break-up at early stages using Lagrangian shell elements to discretize the ammunition hull. Comparison of the observed transient break-up phenomena of both simulations proved that the Eulerian model ensures a sufficient representation of the ammunition casing with respect to its' effects on the flow field. It allows to simulate the full interaction of the gas flow through the expanding fragment cloud in combination with the required numerical stability to a sufficient extend of accuracy. Profound details on the fragmentation itself are not needed, since fragment sizes, speeds and trajectories as calculated using the semi-empirical approach in step 2 of the overall procedure with better confidence and less effort compared to FE approaches.

In the initial phase complex blast phenomena occur. The casings of the individual shells fail, fragments are formed and the expanding explosion products propel the fragment cloud outward at high velocities. The gases escape through the opening gaps of the fragment cloud and a blast wave is formed. For multiple shells a complex interaction process of fragments and expanding waves occur. Figure 6 illustrates this initial phase for a 4 and 16 shell configuration. The red colored material represents the explosive products venting out through the fractured casings. Figure 7 shows the velocities distribution of the 4 shell configuration (0.18 ms after the initiation of the detonation). Where two adjacent explosion and fragment expansions interact on symmetry lines, the so-called 'jetting effect' of increased velocities of up to 2500m/s instead of 1650m/s for single charges can be observed. So with the realized simulation approach it became possible to analyze the differences in the evolution of the detonation process and the resulting loading on the housing structures comparing the cased and uncased charges.

Summarizing, for the cased ammunition a delayed expansion of the shock front is observed. The shape of this front is much more irregular compared to the almost hemispherical expansion of the bare ammunition. For the steel cased ammunition a much stronger directed loading can be observed at discrete locations like at the tip of the charges in the center of gravity (see Figure 7). These focused loading jets result from the break procedure of the casing and lead to a non uniform load distribution on the walls and the ceiling of the surrounding housing structure. The irregularity for the fragmenting ammunition is thereby much more pronounced than for the bare charges, which influences the break-up phenomenology of the housing and the resulting debris throw. Hence, to capture these phenomena within the numerical simulations is essential for the final result of the entire numerical approach.

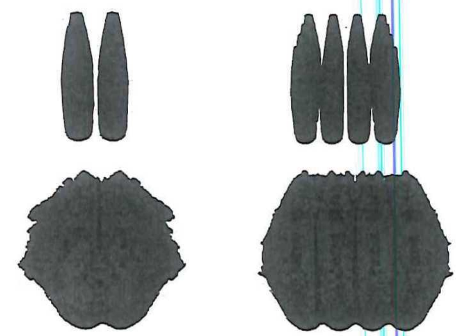

Figure 6 Numerical model of the 4 and 16 shells configuration (top) with break-up and venting of the explosion products (red).

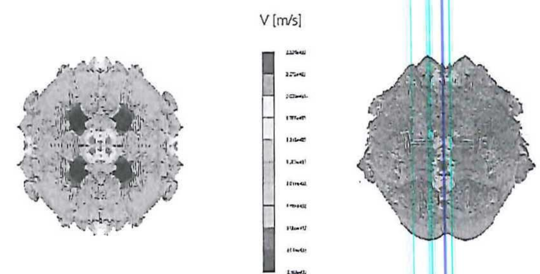

Figure 7 Velocity contours (0-2500m/s) of 4 shells venting through casing during break-up. (Left) top view and (right) 3D-perspective.

2.3. Structural loading and venting

The loading due to an internal explosion consists of multiple shock reflections followed by the gradual build up of the mean "quasi static" gas pressure in the time frame of a few to hundreds of milliseconds. The structural response is also a function of time. Failure mode and failure time depend on the housing dimensions and properties but also on the load amplitude with its' temporal and spatial distribution. For the Kasun structure the strength is overwhelmed by the explosion, especially for the multiple charges, and fails before the gas pressure is fully developed. Therefore the venting process had to be modeled in order to quantify the acceleration of the housing walls and generate the input data for the structural break-up analysis. For this purpose a coarse structural response model for the KASUN significantly increasing. Consequently the application of the latter value would definitely result in higher launch velocities even if the failure mode would be correct.

In the experiments also the internal pressures have been recorded using special carbon gauges. Figure 11 underlines the good agreement of the numerical simulations to the conducted experiments. For the time period in which the experimental gauges did record pressure data in this violent environment the derived curves are very similar and in good agreement to each other.

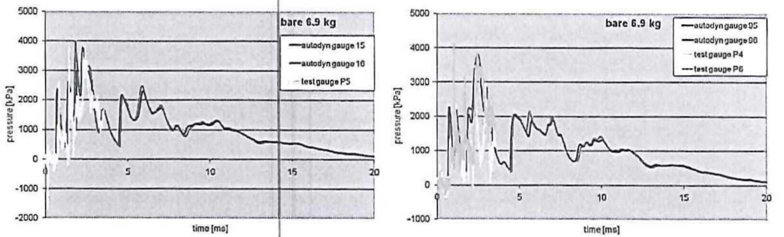

Figure 11 Comparison of the numerical pressure-time histories to the experimental data

Based on these analyses it has been concluded that the 50 % erosion strain is suitable to take the venting of the housing in the numerical simulations into account for all Kasun test conditions with their wide range of loading densities. In addition a time period of 20 ms is sufficient to capture the decisive loading on the Kasun housing before the total break-up in order to determine the appropriate debris launch conditions.

2.4. Results of blast prediction

To capture the irregular spatial load distribution the blast loading was recorded along the wall and roof at 300 gauge points (see Figure 12). These form the direct input for response calculations (section 4.4). In reference [4] the pressure recordings for various locations are presented and discussed. In this paper we only give some examples and mainly the results for the middle of the walls and the mean load values, e.g. Figure 10, Figure 13 and Figure 14.

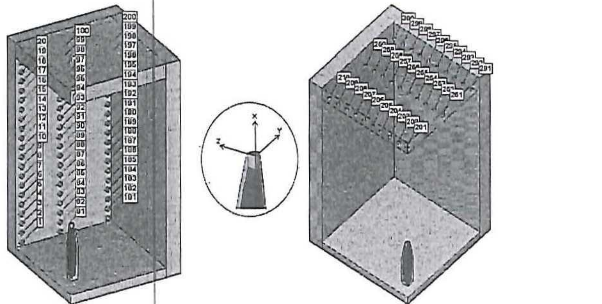

Figure 12 Spatial distribution of gauge points and origin of coordinate systems: 1 to 200 gauge points of the wall, 201 to 300 gauge points of the roof.

In summary the blast prediction showed that:

- The peak overpressure increases with the explosive mass, as expected.
- All bare charge configurations deliver higher peak overpressures than the shell configuration with the same explosive mass.
- The time of arrival of the bare charge configurations is significant earlier than the time of arrival of the corresponding shell configuration
- The 16 shells configuration leads to similar overpressures as the 4 bare charge configuration. 1 bare charge provides peak values similar to the 4 shells configuration.
- The different simulation time is in correlation to the charge mass. For smaller charge masses the break-up and the total destruction of the Kasun housing starts later than for high loading densities.

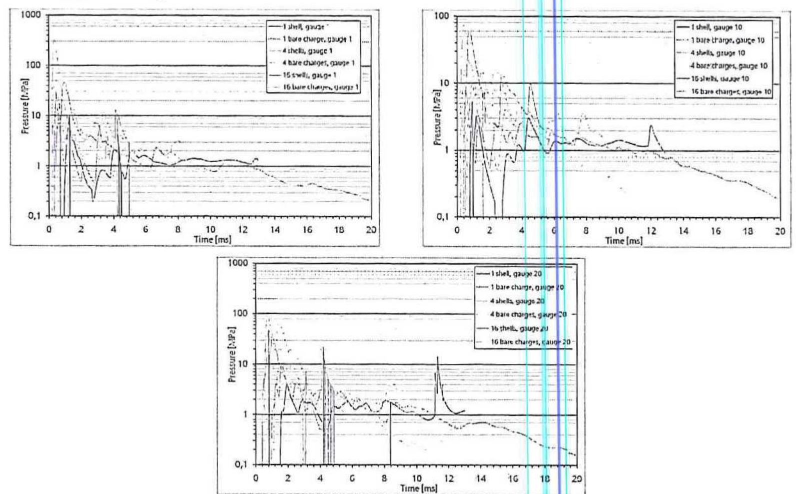

Figure 13 Blast load profiles at node 1 (bottom of the wall), node 10 (at half height) and node 20 (top)

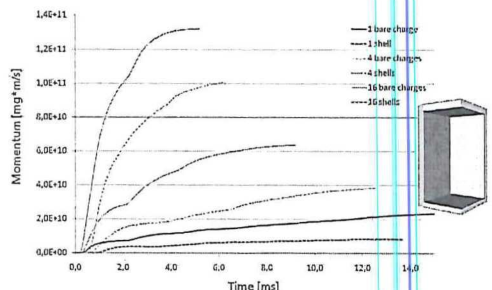

Figure 14 Comparison impulse blast loading on wall for the different charges

To show the differences between the cased and bare charges the impulse loading on the whole wall has been calculated. Figure 14 shows the impulse ratios of the six analyzed charge configurations. All calculations are carried out until the impulse of the wall becomes nearly asymptotic. For the cases with long simulation duration the stability of the calculation is very challenging. As analyzed for the pressure evolution, the 1 shell configuration receives the smallest wall impulse, the 16 bare charge configuration experiences the highest.

In general a smaller impulse is calculated for all shell configurations (without impact of the casing fragments) than for the bare charges. The gradient and the evolution of the curves vary with the configuration.

The numerical model: Step 2 Internal fragment load on RC

3.1. Introduction

The use of available empirical data from arena tests for the fragment mass distribution and the spatial launch velocity distribution of a single shell is the easiest and most reliable way to model the complex debris generation of the shell casing. These were used as input for a combined statistical-analytical approach to determine trajectories of the fragments, deal with fragment collision and calculate the possible impact locations on the different wall sections. The time of flight and the impact impulse were determined for surface areas of 0.2 x 0.2 m^2. The procedure is summarized in this section, details are given in [6] while FE-analyses on the stack effects are reported in [5].

3.2. Fragment mass distribution and launch velocity

The Arena tests of single shells provide detailed information on the fragment mass distribution as well as the spatial distribution of the launch velocities. Figure 15 illustrates the data for a 155 mm mortar shell.

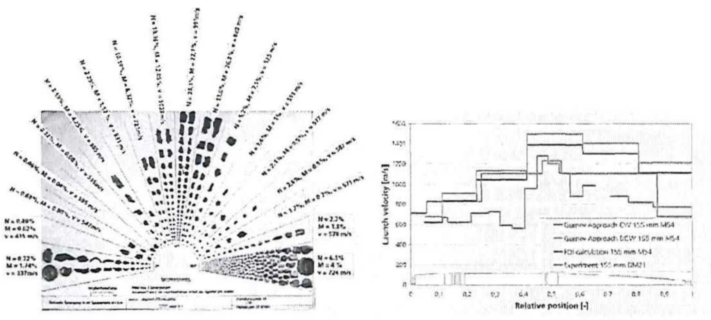

Figure 15 (left) Experimental test results of a detonated 155 mm shell (M107), velocity and fragment mass distribution [7]. (right) Comparison experimental, FE-data and results of the semi-empirical analysis for the fragment velocity distribution.

An upper bound for the launch velocity is obtained with the Gurney approach which provides in combination with a Taylor equation the fragment spatial velocity distribution as depicted in Figure 15 (right). These semi-empirical methods are well established and widely used [8], for more details see [6].

The key issue for our application is how to deal with multiple shells. In the AASTP 1 [9] it is stated that in general larger fragments are expected. This effect is most pronounced for ammunitions with small charge to metal ratios such as artillery shells. Another aspect is that the velocity of the leading fragments from a stack of projectiles has been observed to be as much as twice the value of a single shell by the 'jetting effect'. To get more insight in the interaction process between the failing shells a numerical study of the stack effect was performed [5]. The main result of the investigation is shown in Figure 16. The fragments of the outer corner shells attain a similar velocity in comparison to the velocity of single shell fragments. Significantly higher velocities are observed especially in the 16 shell stack configuration, when the fragments are emitted in the direction of $r_{2,1}$ and $r_{2,2}$ at about half of the shell height.

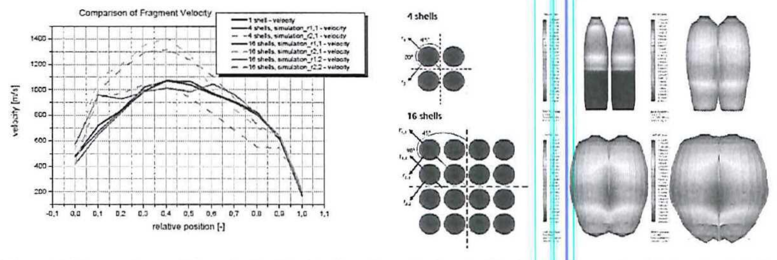

Figure 16 Comparison of the velocity distribution along the longitudinal axis of a stack with 4 and 16 shells to a single 155 mm M54 shell and an illustration of the deformation sequence in stack of 4 shells.[5]. A velocity increase of up to 40% by the stack effect is observed

In spite of these stack effects on the launch velocities it was decided that, in this phase of the study, the single shell data would be used as a reasonable approximation (black curve in Figure 16.

3.3. Fragment propagation model

With the above mentioned fragment and launch data a fragmentation propagation model was developed. In this model each individual shell is modeled as a point source in 3D space at half height of the actual shell. The effect of a warhead is simulated by launching a defined number of representative fragments [10]. As depicted in Figure 17 the fragments of the experimentally determined fragment matrix are distributed and launched on representative directions in a local coordinate system which is defined by the deposition angle of the warhead and the location at detonation. The surface of a unity sphere around the warhead is therefore subdivided into windows of approximately equal size. The probability that a fragment of a mass class is launched in a specific direction through the middle of a window is calculated. It gives the average number of fragments that are launched through a specific window on the unity sphere. In the model the fragments are conservatively launched with the maximum mass of the associated mass class and maximum velocity in the corresponding spatial orientation. Because of the short flight distance to the walls and ceiling gravity and drag are neglected in the trajectory calculations. In case of the four and sixteen shell configurations fragment collisions are considered within the developed computer routine. The problem was simplified by assuming full plastic collision, so the equations could be solved analytically and the post impact fragment mass and velocity vector is known. This approach was programmed in a model providing the fragment impact data on the structure. The data consists of the number of fragments hits per mass class, the corresponding velocities and the arrival time. The number of hits is "weighted" by the probability number that the fragment is launched through the corresponding window of the point source (see Figure 17). To provide the fragment loading data for the response calculations the impact data is sampled for wall-areas of 0.2 x 0.2 m^2. Figure 17 (right) gives examples of the calculated hit locations and impulse density plots on a wall for the 4 shell stack.

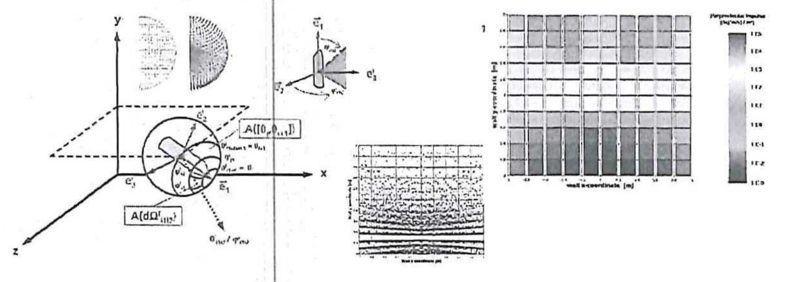

Figure 17 Representative directions of launch for warhead fragments (left). Modelling results 4 shell stack, impact locations on wall (middle) impulse density distribution along on wall (right).

The numerical model: Step 3 Response calculation of RC housing

4.1. Introduction

The finite element simulations of the third stage have been performed using LS-DYNA. It should be noted that the simulation of the structural response up to failure, the break-up of the RC-structure under the severe dynamic loading is extremely challenging. It is at, or probably beyond the possibilities of the (commercial) numerical codes available. The temporal and spatial gradients in the stress and deformation fields are high, especially when concrete fails, which leads to numerical instabilities. Although we knew these challenges in advance, it was decided to explore and use the possibilities of detailed computational modeling in order to learn about the sequence of loading and response phases and spatial and temporal energy distributions.

The objective of the simulations is to get insight into the influence of the fragmenting casing on the response, the break-up and the debris launch conditions. Therefore the structural response is modelled stepwise. In each step, a load/response parameter is changed or added. Four response analyses have been performed, i.e. due to (i) bare charge blast, (ii) blast of cased shells, (iii) blast and fragment pulses from cased shells and (iv) response and erosion under blast and fragment pulses from cased shells. Full description of the modeling and the analyses of the results are given in [11, 12]. In this chapter we focus on how we dealt with the fragment loading, summarize the response results and compare these briefly with experimental data.

4.2. Fragment loading from shell casings

The casing fragmentation model discussed in the previous section, provides for the thousands fragments not the hit location of each individual fragment but, for all fragments, the probability to find a fragment in a given region. To determine the damage and response process of all the fragments, the entire structure would have to be modelled in great detail. This is not feasible from a numerical point of view within a reasonable computer time. Hence, a more efficient 'bottom-up' approach has been developed using all the available information and making simplifying steps when necessary.

The strategy is as follows, first the penetration of individual fragments is considered. For the defined fragment mass classes and range of impact velocities, the penetration depth was determined with detailed FEM simulations, compared with semi-empirical relations and represented in a penetration depth ($d(\phi,v)$) curve. A second order polynomial has been assumed [$d(\phi,v) = A_1\phi v^2 + A_2\phi^2 + A_3\phi v + A_4$] and the constants are obtained from the FEM simulations using a least squares fit.
Next the pressure pulse of the fragments is determined. From the penetration simulations the deceleration force and penetration time can be derived, but we preferred to schematize the problem as follows. The fragment impulse ($m_i.v_i$) is known as input. By assuming a constant impact load during the penetration time Δt and a constant deceleration of the fragment (as observed in the FEM analyses), also the load amplitude is known. The spatial-time distribution of the fragment impacts on the Kasun structure is given by the fragment model. The walls and roof were divided in square region (A_s) of 10cm by 10cm squares (see **Figure 20**). In each square region, a number of fragments may impact, with different impact probability (ω_i). According to this schematization the pressure (p_i) transferred by a fragment (i) is: $p_i = \omega_i m_i v_i^2 / 2A_s d_i$. The spatial and temporal distribution of the fragment pressure pulses were determined and added to the blast load. In this phase of the study only the velocity component normal to the wall or roof was taken into account.

The third preprocessing step to get the dominant effects of the fragment impacts as input for the structural response calculations is the erosion of the concrete by the fragments. At forehand it was not known what the effect could be, so we decided to include the effect. As a first approximation, the erosion volume is computed based on the penetration depth (d_i) and the fragment diameter (ϕ_i). Since only entire fragments should be considered, the fragments with the highest impact probability are selected, such that their accumulated momentum coincides with the average momentum.

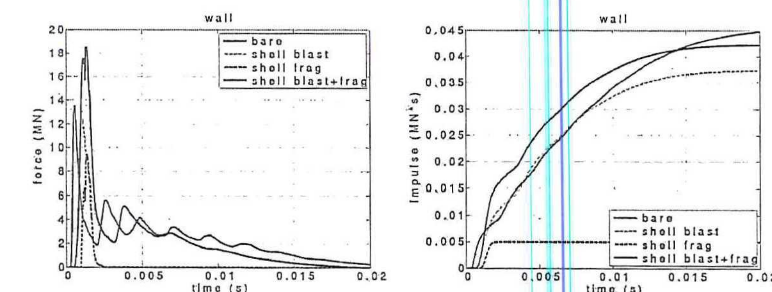

Figure 18 Single charge, bare and shell. Force and total impulse history on ½ wall bare charge; (green) shell blast; (black) fragment load; (blue) shell charge

4.3. Results of the blast and fragment load predictions

The models and procedures described in the previous sections provide the spatial and temporal distribution of the load on the structure. To illustrate the casing effects on the overall loading on the walls, we give and discuss in this section the total force and momentum as function of time.

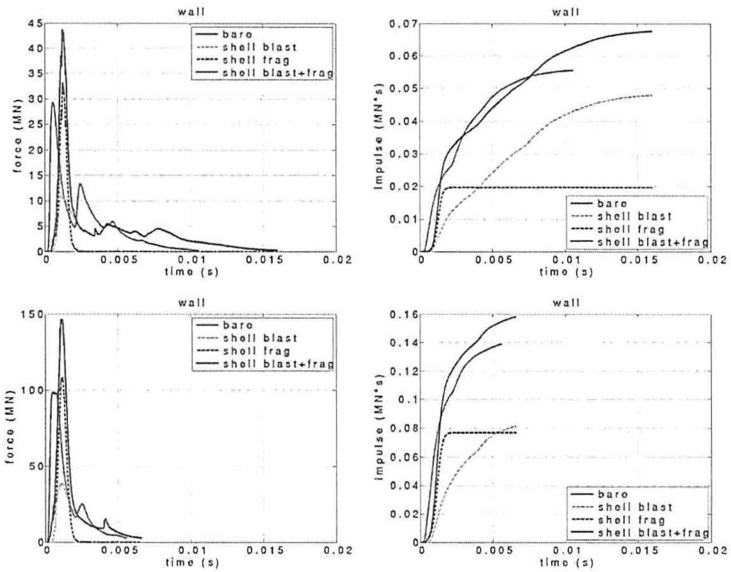

Figure 19. 4 (top) and 16 charges (bottom), bare and shell. Force and total impulse history on ½ wall. (red) bare charge; (green) shell blast; (black) fragment load; (blue) shell charge

Some observations:

- The maximum force and maximum impulse on the wall is higher for cased charges than for the bare charges, except for the single charge. For the single charge, the main pulse of fragment impact arrives slightly after the blast shock front causing a double-peak in the combined loading (). For the 4 and 16 shells the pulses coincide, see Figure 19.
- For the cased charge the load arrives slightly later than for the bare charge but increases much faster. The result is that the impulse for the cased charge initially exceeds the blast of the bare charge but finally, after about 15 msec, the impulse of the bare charge is higher.
- For both single charge tests, the duration of the loading is about 20 msec. The situation changes for the multiple charge tests. Not only the load duration is shorter for the higher charge weights, but there is also a clear difference between the bare and cased tests. Venting due to failure of the structure occurs at a more early phase for the higher charge weights. It occurs also sooner (at 10 msec) in the test with the bare charge test than with the cased charge (at 16 msec). A similar effect is seen for the 16 charges, but less distinctive and at shorter times (5 msec). For the tests with multiple cased charges only a part of the blast energy is transferred to the structure while the full fragment impact energy is transferred.

For the cased charges, the contribution of the fragments to the force on the walls is very significant, and this effect increases with the number of shells; whereas the fragments contribution to the total force on the roof is negligible.

4.4. The numerical structural model

The concrete target, as described in section 2.1, is modeled using 8 noded solid elements, with reduced integration, and the K&C damage concrete material [13]. Rebars are modelled using beam elements and elasto-plastic material model with kinematic hardening. The floor is modelled as a rigid material. Due to symmetries, only one quarter of the structure is modelled. The floor nodes are constrained in all directions.

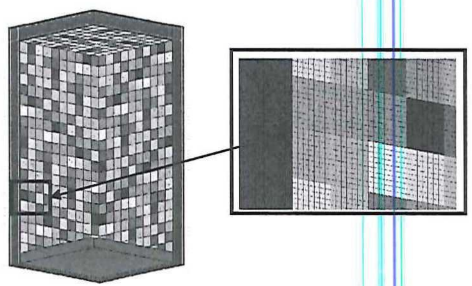

Figure 20 Shell parts 10 x 10 cm with uniform pressure

To transfer the blast and fragment load to the structure, shells with zero strength and no mass are defined on the internal wall and roof surfaces. These shells are grouped in square regions of 10cm by 10cm where a uniform pressure is applied (see colored areas in Figure 20). The average element length is 15 cm. The complete computational model contains 480196 concrete solid elements, 20196 rebar beams and 32900 shells.

4.5. Notes on element erosion

In this section we want to highlight the critical issue of element erosion for the break-up modelling. It is used (i) to remove fully softened and strongly deformed elements. A shear strain of 0.5 is used and (ii) to account for shell fragment impact erosion.

Due to the severe blast and impact loading high spatial and temporal stress and deformation gradients occur. The damage will not develop smoothly but very irregularly. Computationally, convergence and stability problems occur. The common strategy is to "erode" (=delete) those elements in which the material failed and deformed to the degree that stability problems are introduced. Erosion of elements should only happen when the considered element does not play a role on the global response anymore, because its'energy and momentum is deleted from the system and for concrete (non-isotropic in failure) the resistance of the structure might be reduced too much. The strategy is to set the stiffness and strength in the direction of failure to zero, and only at a predefined threshold of deformation the element is eroded.

Obviously the element erosion coupled to the fragment penetration increases with the number of cased charges (shells). Most fragment impacts take place at the bottom of the walls, followed by the centre of the roof. In the single-shell case, only a few fragments perforate the concrete wall. In the four-shell case, many fragments perforate the concrete walls. The effect is more expressed for the sixteen-shell case. In this case, the number of fragments is so high that the erosion volumes of each fragment overlap. It is clear that the validity of the procedure of damage due to individual impacts is highly questionable. By the large number of eroded elements the wall structure gets an irregular and porous geometry (see **Figure 21**) leading to additional numerical instability challenges.

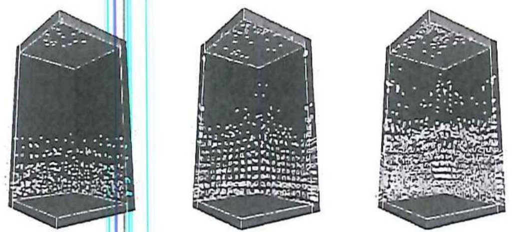

Figure 21 Eroded volumes due to representative fragment impacts. Inside view for 1, 4 and 16 shells

In this paper the shell simulations do not include fragment impact induced concrete erosion, and only the fragment impulse is accounted for.

4.6. Results response simulations

The response simulations provide the deformation and failure process of the structure as a function of time. The time sequence, the launch conditions of the debris and the energy distribution are presented and discussed in [12]. In this paper we limit ourselves to the output that can be compared to the experimental data, i.e. the launch velocity and the launch angle.

To give an impression of the failure mode of the Kasun structure for the different loading conditions, the deformed shape for all 6 cases (1, 4 and 16 bare charges; and 1, 4 and 16 shell charges) is shown in Figure 22, at the same time t=7 ms.

Figure 22 Deformed shape at t=0.007 s.;(left) set 1 charge; (middle) set 4 charges and (right) set 16 charges; per set (left) bare charges right) cased charges

We see that the deformations are larger for the bare charges than for the cased charges, especially for the 4 and 16 shell tests. For the cased charge tests the impulse on the walls at t = 7 msec walls is higher (1 and 16 charges) than or equal (4 charges) to the impulse in the bare charge tests (see sections on Step 1). Nevertheless the deformations are larger for the tests with bare charges. This can be explained by the different spatial and temporal load distribution. For the cased charges the fragment loading is mainly directed to the lower part of the structure which might be less effective for structural failure than the more "equally distributed" blast load. For the bare charges the blast load is higher and arrives earlier in time. Venting, blast release, occurs sooner and is more pronounced in the bare charge tests than in the cased charge tests.

The numerical simulations also show that there is a clear difference in launch angle for the bare and cased charge tests, see Figure 24 for single charges. Also for multiple charges counts that the launch angle is lower (almost horizontal) for the cased charges than for the bare charges. To illustrate the different deformation shapes, the results for the 16 charge tests are compiled in Figure 23. These observations correspond to the experimental findings. [14]

According to the calculations, the structure does not disintegrate in the initial phase. So, the structural response influences the launch conditions of the debris. For the 16 charge-tests the sequence of failure at the top and bottom corner is different for the bare and cased charges. Evaluating these results we have to realize that a continuum damage model is used and elements are eroded only after a shear deformation of 50%. Discrete cracking is not modeled and the break-up process is represented phenomenologically on a macro-scale only. In spite of all discussed limitations of the the computational results, we state that (i) the initial load distribution and (ii) the early time response and damage development have a significant influence on the debris launch angle. Consequently, structural properties and design as well as the charge configuration will influence at least the launch angle. It should be noted that in the "clamped plate tests" the KG performed in the past, we also saw that the plates did not disintegrate in the early phase. In spite of severe cracking and deformation, disintegration was not observed for a flight distance of at least a quarter of the span width [15].

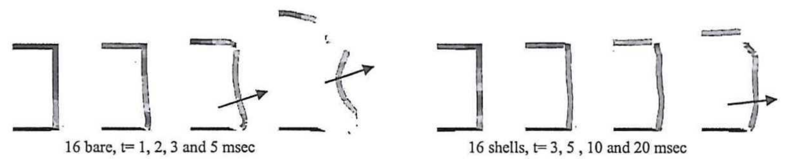

Figure 23 Vertical cross section along symmetry plane, deformation and launch sequence for 16 charge-tests

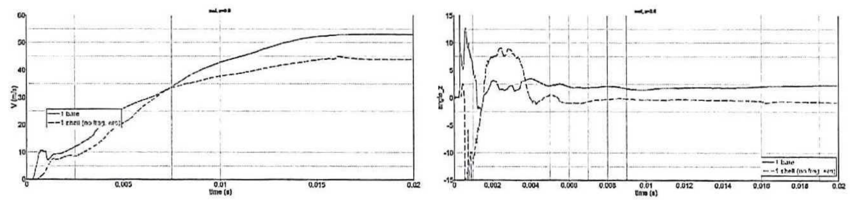

Figure 24 Example velocity (left) and launch angle history (right) at 0.6 m height, 1 bare (blue line) versus 1 shell charge (red line), see for the corresponding load profiles Figure 18.

The predicted launch conditions (velocity and angle) correlate reasonably with the experimental data. To illustrate this, the launch velocity data is compiled in Table 2.

The numerical results were also used to investigate the energy distribution and quantified the (i) kinetic, (ii) internal, (iii) hourglass, (iv) eroded kinetic and (v) eroded internal energies as a function of time. The results [12] show that most of the energy is kinetic, followed by the internal energy while the numerical artifacts of hourglass and eroded cells' energies are negligible. The ratio E_{kin}/E_{def} ranges from 8 to 40 for the single and the sixteen charges resp. The fact that the maximum hourglass energy is only a few percent of the energy in the structure, shows that no artificial solutions are obtained.

Table 2

Test	V_{test} (mean) [m/s]	V_{test} (min) [m/s]	V(simulations) [m/s]
1 bare/	52	29	53
1 shell/	38	26	44
Ratio bare/cased	**1.37**		**1.21**
4 bare			72
4 shell			56
Ratio bare/cased			**1.28**
16 bare/	224	173	167
16 shell/	165	74	111
Ratio bare/cased	**1.36**		**1.50**

Concluding remarks

EMI and TNO successfully developed a three step procedure to determine the blast loading, the fragment loading and the response and break-up of RC structures due to internal explosions. It is a balanced procedure in which advanced numerical techniques and models are combined with semi-empirical models to capture physics as good as possible and to minimize the introduction of uncertainties.

Modeling the whole process of detonation up to the break up of RC structures is at or beyond edge of commercial codes. The explosion conditions with multiple fragmenting shells were simulated using coupled, multi-material hydrocodes for the flow field (stage I) and semi-empirical for the fragment propagation trajectory calculations (stage II). Both local pressure-time histories and average fragment impact momentum were then load conditions for the response of the RC housing (stage III)

The simulations predict higher velocities, higher kinetic and higher internal energy for the bare charge tests, while the impulse at the wall is higher for the shell tests. The spatial and temporal load distributions have a significant effect on the failure of the structure. To determine the debris launch conditions loading and response have to be coupled in the calculations.

In spite of observed limitations the developed 3-step approach can be used to determine the initial launch conditions of the debris throw for bare as well as cased charges. Simple analytical formulae to take into account cased charges based on the available engineering approaches for uncased charges in RC-structures are the aim of the KG research project. Comparison with experimental data showed good correspondence, so the method can be used to extrapolate test results to other explosion scenarios.

Acknowledgement: The authors gratefully acknowledge the important technical contribution by Martin Voss on shell fragmentation modeling and Lars Mitzka and Simon Vetter on FE blast simulations. This project was funded by the Klotz Group an international group of experts on explosion safety, representing the USA, UK, D, No, Swe, CH, NL and Sin.

REFERENCES

[1] Century-Dynamics (2005). AUTODYN Theory Manual. Revision 4.3.

[2] Herrmann, W. (1969). Constitutive equation for the dynamic compaction of ductile porous materials. J. Appl. Phys. 40: pp. 2490–2499.

[3] Johnson, G. R. C., S. G. (1983). A constitutive model and data for metals subjected to large strains, high strain rates, and high temperatures. 7th Int. Symp. on Ballistics, The Hague, The Netherlands.

[4] Stolz, A. (2010). Simulation of Pressure Evolution during venting in the Kasun Houses. EMI report I-08/10

[5] Vetter, S.(2008). Klotz Group Engineering Tool – Effect of Cased Ammunition. Report 19/08, Freiburg: Fraunhofer-Institut für Kurzzeitdynamik, Ernst-Mach-Institut.

[6] Dörr, A., Voss, A. and Pfanner, T. (2008). Analytical Investigation of the Stack Effect, Resulting Ammunition Fragment Spatial Mass,Velocity and Angular Distribution. Report I-20/08 Fraunhofer Ernst-Mach-Institiut

[7] WTD91 Velocity and fragment mass distribution of a M107 shell. Meppen, WTD91.

[8] Methodologies for calculating primary fragment characteristics«;Technical Paper No. 16 Revision 1; Department of Defense Explosives Safety Board; Alexandria VA; 2003

[9] Manual of NATO Safety Principles for the Storage of Military Ammunition and Explosives«; Allied Ammunition Storage and Transportation Publication; AASTP-1 Edition No.1; 1997

[10] Grundlagenstudie zur Überflugsicherheit: Physikalische Beschreibung der Splittergefährdung«; I. Häring; Fraunhofer-Institut für Kurzzeitdynamik, Ernst-Mach-Institut; E 04/05; Januar 2005

[11] Mediavilla Varas, J. and Doormaal, J.C.A.M. van. (2009). Klotz group engineering tool - Effect of cased ammunition. WP3 - Modeling damage and response of Kasun structure. Report TNO-DV 2009 C197

[12] Mediavilla Varas, J. and Weerheijm, J. (2011). Simulations of damage and response of KASUN Houses. WP3 The effect of cased ammunition. Report TNO-DV 2011 C110.

[13] Hallquist, J.O., LS-DYNA keyword's user manual, version 971. (2007): Livermore software technology corporation.

[14] Grønsten, G.A, Berglund, R., Carlberg, A. and Forsén, R. (2009) Break up Tests with Small "Ammunition Houses" Using Cased Charges - Kasun III, Report FOI-R-- 2479 –SE ; Forsvarsbygg Report 68/2009 ISSN 1650-1942

[15] Lim, H. S. and Weerheijm, J. (2005) Break-up of RC-slab due to internal explosion. Proceedings ISIEMS 2005.